Stateselected photodissociation dynamics of HONO(Ã1 A'): Characterization of the NO fragment

R. N. Dixon and H. Rieley

Citation: The Journal of Chemical Physics **91**, 2308 (1989); doi: 10.1063/1.457038
View online: http://dx.doi.org/10.1063/1.457038
View Table of Contents: http://scitation.aip.org/content/aip/journal/jcp/91/4?ver=pdfcov
Published by the AIP Publishing

State-selected photodissociation dynamics of HONO ($\tilde{A}\,^1A''$): Characterization of the NO fragment

R. N. Dixon and H. Rieley[a)]
School of Chemistry, The University of Bristol, Bristol BS8 1TS, United Kingdom

(Received 27 February 1989; accepted 5 May 1989)

Trans-HONO has been photodissociated through the 2_0^2 band of the $\tilde{A}\,^1A''$–$\tilde{X}\,^1A'$ system at 355 nm. The energy disposal in the NO fragment, and vector correlations between its motions, have been characterized using polarized one-photon excited laser induced fluorescence. The rotational distribution, rotational alignment, degree of electron alignment, spin–orbit branching ratio, approximate vibrational distribution, and energy partitioning are determined. The rotational distributions in each of $v(\mathrm{NO}) = 3,2$ and 1 are highly inverted and approximately Gaussian in quantum number. The peak J decreases with increasing v to give a fairly narrow overall internal energy distribution. The disposal of the available energy into all NO and OH motions is 60% and 40%, respectively, and is also 40% into internal motions, mainly of NO, and 60% into translational recoil. The NO rotation shows a positive alignment. All the vector correlations are consistent with planar fragmentation dynamics, but with a finite dissociation lifetime of about 100 fs. The Λ-doublet populations of NO indicate the preference of the unpaired π electron to occupy an orbital lying perpendicular to the plane of rotation, which is opposite to that found earlier for the OH fragment. The population of the NO spin–orbit states is inverted. These results are discussed in terms of dynamical models and the features of a recently published *ab initio* surface for the HONO $\tilde{A}$ state.

I. INTRODUCTION

Recent advances in the photodissociation of polyatomic molecules have highlighted two extremes for the distribution of the available energy over product motion; namely, those cases where the energy becomes statistically distributed over all possible product states, and those exhibiting specific dynamical control. In the second class vector correlations provide valuable information additional to that from product distributions in separating the effects of the initial state of parent preparation from exit-channel recoupling during motion over the excited state hypersurface.

HONO in its first excited $^1A''$ state is known to dissociate with unit quantum efficiency to give two products in $^2\Pi$ states:

$$\mathrm{HONO}(\tilde{X}\,^1A') \xrightarrow{310\text{–}390\,\mathrm{nm}} \mathrm{HONO}(\tilde{A}\,^1A'') \rightarrow \mathrm{OH}(X\,^2\Pi) + \mathrm{NO}(X\,^2\Pi) \quad (1)$$

The OH ejected by this half-reaction has already been completely characterized by sub-Doppler and polarization laser spectroscopy.[1,2] The OH fragment was found to be translationally hot ($\sim$0.5 eV) with a nearly $\sin^2\theta$ angular distribution about the electric vector of the photolysis laser. The corresponding shapes of the lines in the OH A–X laser induced fluorescence (LIF) excitation spectrum are Doppler split. The internal motion of the OH fragment is vibrationally and rotationally cold. The spin–orbit components and the Λ-doublet components are not in equilibrium. The OH rotation is aligned, and the π lobe of the unpaired electron lies preferentially in the plane of rotation. Both of these effects become more pronounced with increasing OH rotational excitation.

These observations have obvious implications for the hitherto unobserved NO fragment, which is predicted to be formed with a large degree of internal excitation, and anisotropic behavior. This paper presents an investigation of these predictions by completely characterizing the NO fragment. Taken together, these two sets of results permit a full description of the photodissociation dynamics of this tetratomic prototypical nitrite.

The earlier OH study was carried out using samples of HONO generated in equilibrium by the surface-catalyzed reaction between NO, NO_2 and H_2O at room temperature[3]:

$$\mathrm{NO} + \mathrm{NO_2} + \mathrm{H_2O} \rightleftarrows 2\mathrm{HONO}. \quad (2)$$

This method is not suitable for investigation of the NO photofragment because (i) the equilibrium concentration of HONO is low compared with that of NO, and (ii) NO_2 photolyzes to yield NO at all wavelengths within the HONO absorption band. The prediction that the desired NO photofragment would be rotationally hot suggests the use of jet-cooled samples to remove interference from the equilibrium NO. Unfortunately our observations on the character of the fragment spectra have shown that HONO clusters extensively under such conditions. The success of the present work has therefore hinged on maximizing the ratio of HONO to NO and NO_2 (and also N_2O_3 and N_2O_4).

The HONO absorption spectrum between 310 and 390 nm is dominated by the progression 2_0^n in a vibration localized in the terminal NO bond of the *trans* tautomer.[4] The third harmonic of a Nd:YAG laser (355 nm) falls within the 2_0^2 band, for which the available energy (11 650 cm^{-1}) is sufficient to populate NO states up to $v'' = 6$. In contrast,

[a)] Present address: Department of Chemistry, University of Toronto, Toronto, Ontario M5S 1A1, Canada.

 0021-9606/89/162308-13$02.10

from NO_2 only $v''=0(J''\leqslant 44.5)$ and $v''=1(J''\leqslant 29.5)$ are accessible at this wavelength. Thus NO in $v''\geqslant 2$ can be unambiguously attributed to HONO photolysis, but allowance must be made for a possible NO_2 precursor for the lower NO states. The experiments reported in this paper are restricted to this single photolysis wavelength.

II. EXPERIMENTAL

A. Sample preparation

The method which was found to yield satisfactory concentrations of HONO and minimal amounts of NO_2 was similar to Method Ia of Kenner *et al.*,[5] and one with which it is possible to obtain a concentration of HONO greater than the equilibrium value.[6,7] It is the reaction of aqueous $NaNO_2$ and dilute acid at 0 °C:

$$2NaNO_2 + H_2SO_4 \rightleftarrows 2HNO_2 + Na_2SO_4. \qquad (3)$$

Unfortunately this reaction does not yield pure HONO as competing reactions produce large quantities of NO and a trace of NO_2, especially on warming.[8] For each preparation, 200 cm^3 of 0.1M $NaNO_2$ and 100 cm^3 of dilute H_2SO_4 (10% by volume) were maintained at 0 °C using an ice bath and degassed under vacuum before mixing. After addition of acid (under vacuum), nitrous fumes produced *in situ* were exhausted through the experiment reaction chamber in a continuous effusive flow. All surfaces in contact with the nitrous fumes, before the vacuum chamber, were coated with PTFE (Vdax 550 fluorotelomer) in order to inhibit the surface catalyzed equilibrium back to NO_2, NO and H_2O. It was important to maintain a low concentration of NO_2, to avoid detection of NO in high vibrational states with the probe laser alone. Under these conditions no trace of the characteristic brown color of NO_2 was visible in the 500 cm^3 mixing bulb.

B. Apparatus

The experimental configuration adopted was a traditional coaxial geometry for LIF probing. Briefly, photolysis and probe laser beams were counterpropagated coaxially through a vacuum chamber into which the HONO sample was introduced. NO fluorescence was detected by a solar blind photomultiplier (PM:Hamamatsu R166) at right angles to both the molecular flow and the path of the beams. A Nd:YAG (JK Lasers HY-750) was the pump source for both the photolysis and probe light. The former was the third harmonic at 355 nm: for the latter, Raman shifting, in H_2, the doubled output of the dye laser (Quanta-Ray PDL-1) pumped by the second harmonic (532 nm) generated UV probe radiation at the appropriate one-photon energy. A Pellin Broca prism (PB) provided wavelength separation of the Raman orders and a home built autotracking device maintained the optimum phase-matching angle of the KDP doubling crystal. Both beams were linearly polarized and the plane of polarization of the photolysis light ($\hat{\epsilon}_p$) could be rotated through 90° by adjusting the optical configuration. The photolysis beam (<5 mJ pulse energy) was unfocused and slightly divergent through the reaction chamber resulting in a beam diameter in the interaction region of ~ 5 mm. The probe radiation (of polarization $\hat{\epsilon}_a$) was attenuated with neutral density and UV transmitting (Schott UG-5) filters to achieve a pulse energy of less than 10 μJ in the chamber and a beam diameter of ~ 2.5 mm, thereby avoiding saturation. At this power density the fluorescence signal was approximately linear in probe power, which was monitored using a photodiode (PD). The time delay between photolysis and analysis was determined by the difference in optical path length of the two beams and was ~ 10 ns. The dye laser bandwidth (~ 0.6 cm^{-1}) could be narrowed with an intracavity etalon giving a bandwidth of ~ 0.07 cm^{-1} in the visible which was pressure tuned using Ar gas. The calibration in this mode of operation was the synchronous recording of the LIF excitation spectrum of I_2, whose spectral frequencies are well documented.[9]

The stainless steel reaction chamber was fitted wth baffle arms, coated in matt black, in order to reduce scattered light. An effusive flow of the HONO sample was introduced into the chamber through a pyrex capillary, centered in a 1 in. diameter tube, which terminated in a spherical bulb (~ 1 cm diameter) pierced with radial pinholes (~ 1 mm diameter). The position of the end of the capillary was adjustable and was usually set ~ 1 cm from the path of the laser beams through the baffle arms. Baffled fluorescence collection optics were situated ~ 5 cm above the point of intersection of the beams and the gas flow. The chamber was evacuated with a rotary pump and the gas flow was throttled in order to maintain an ambient pressure of 100–150 mTorr (1 Torr = 101 325/760 Nm^{-2}) as measured by a Pirani pressure gauge in the backing line.

NO fluorescence in the range 225–260 nm was detected by the solar-blind PM, which accepted all polarizations equally. The signal was processed through a linear gate (Stanford Research Systems SRS-250) and terminated into 50 Ω in order that detection of scattered light could be avoided by setting an appropriate delay. An apple II microcomputer displayed and stored the digitized NO spectra and probe power and additionally, in the case of etalon scans, I_2 spectra and pressure variation.

C. Procedure: Broad-band scans

The recording of complete scans of the NO(v'–v'') bands was complicated by several factors: (i) the deflection by the Pellin–Broca prism varied with wavelength causing beam walk, eventually leading to misalignment of the two laser beams and an artificial falloff in both fluorescence intensity and recorded power; (ii) the concentration of HONO did not remain constant over the time scale of each experiment, and (iii) the bands were extensive, covering several nanometers (~ 4 nm at the UV wavelength) and were highly structured. In order to achieve adequate resolution data points were collected at ~ 0.5 cm^{-1} intervals. These factors precluded the uninterrupted recording of a complete band (~ 750 cm^{-1}).

In order to circumvent all of these problems broad-band spectra were recorded in sections each covering ~ 1.2 nm in the UV and adjacent sections were overlapped by ~ 0.2 nm. Typically six sections were required to cover a complete band. Prior to each scan the probe alignment was fixed at the midpoint of the range by adjustment of the PB. The angular

variation of the probe beam emerging from the PB was only $\sim 0.025°$ over each scan, corresponding to a displacement of the beam in the interaction region of ~ 0.2 mm and this was observed not to affect the recorded fluorescence intensity or the recorded power level. The latter was the more sensitive to misalignment and it was found that reducing the beam size of the face of the PD using a short focal length lens ($f = 10$ cm) minimized this. A fresh nitrite/acid solution was prepared for each set of scans. The variation of HONO concentration with time was monitored by measuring the intensity of a chosen strong NO spectral feature at the beginning of each experiment and following every scan. For each measurement the PB was adjusted for optimum probe alignment. Zero levels of fluorescence signal and power were noted for each scan to permit future normalization. The time taken to record a whole band in this way was ~ 2 h. Bands were recorded in both increasing and decreasing wavelength and at two different relative polarizations of pump and probe laser: H_p,H_a (Geometry I) and V_p,H_a (Geometry II), where H and V refer to horizontal and vertical polarization respectively, i.e., H_p implies detection along $\hat{\epsilon}_p$ and V_p implies detection perpendicular to $\hat{\epsilon}_p$. Each was repeated to confirm reproducibility.

Spectra recorded in this manner were transferred to a mainframe computer where they were separately power normalized and corrected for any falloff in HONO concentration with time (assumed linear between measurements) and then spliced together. The continuity of power over the complete band could be checked on the composite spectra and its variation reflected the dye gain curve over the region.

D. Etalon scans

Regions of approximately 10 cm^{-1} in the UV were scanned by pressure tuning with Ar an intracavity etalon. The midpoint of each scan was positioned at the peak of an etalon mode by viewing the ring patterns through a handheld etalon and telescope. Scans were overlapped by offsetting the dye laser grating by four etalon modes at a time. The HONO concentration was assumed constant over each scan and each spectrum was power normalized and linearized to the variation of the cavity pressure.

III. RESULTS AND DATA REDUCTIONS

A. Broad-band spectra

Complete sets of spectra in Geometry I (H_p,H_a) and Geometry II (V_p,H_a) were recorded for the NO(0–2) and NO(0–3) bands following 355 nm photolysis of HONO. The (1–4) and (1–5) bands were used in an attempt to probe $v'' = 4$ and 5, respectively, as these had higher transition probabilities than the corresponding (0–4) and (0–5) transitions.[10] No population, above the level of the noise, was detected in $v'' = 4$ or $v'' = 5$. NO detected in $v'' = 1$ via the (0–1) band was dominated by NO from the dissociation of NO_2, with contributions from both thermal NO and NO from the dissociation of HONO. The latter is clearly distinguished by transitions occurring at high J. An extensive survey of the (0–0) band was not undertaken as it is dominated by thermal NO with a significant detectable population at high J, and a highly inverted NO rotational distribution from the NO_2 dissociation.[11]

Figure 1 shows a power normalized and concentration corrected composite spectrum of the NO(0–2) band taken with the relative polarizations of the photolysis and probe laser beams being $\hat{\epsilon}_p \| \hat{\epsilon}_a$ (Geometry I). Immediately apparent is the highly inverted and extensive rotational excitation and transitions occurring from $J \sim 49.5$ were clearly visible. The absence of the familiar bandhead structure so prominent in the spectra of Boltzmann-like distributions indicates a low population in low J'' states. Comparison of this spectrum with that taken in Geometry II shows small but significant differences in relative branch intensities, consistent with rotational alignment of the NO fragment.

The effects of alignment are more easily recognized by comparing small sections of an appropriate spectral region, especially in the NO(0–3) band where linewidths are narrower. The low resolution spectra due to $v'' = 3$ look qualitatively similar to those of $v'' = 2$, in that they display the same inverted and extensive rotational distribution. Figures 2(a) and (b) show an assigned narrow region of the (0–3) band at the longer wavelength end of the spectrum. The effect of changing the relative polarizations of the beams from $\hat{\epsilon}_p \| \hat{\epsilon}_a$ (Geometry I) to $\hat{\epsilon}_p \perp \hat{\epsilon}_a$ (Geometry II) is to cause an inversion in the $Q_{22} + R_{12}$ and $P_{22} + Q_{12}$ intensities. The former,

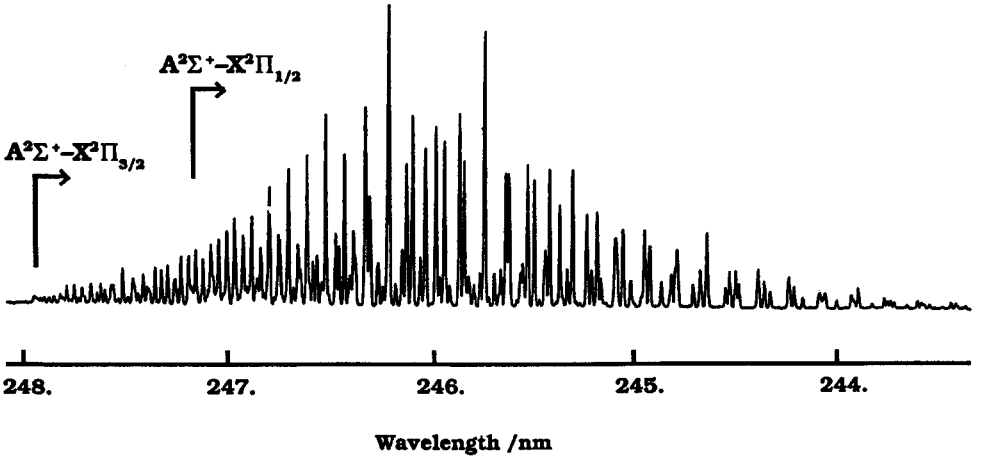

FIG. 1. An LIF excitation spectrum of the NO(A–X) 0–2 band following photolysis of HONO at 355 nm. This spectrum was recorded in Geometry I, with $\hat{\epsilon}_p \| \hat{\epsilon}_a$. Note the absence of pronounced band heads because of a highly inverted rotational distribution.

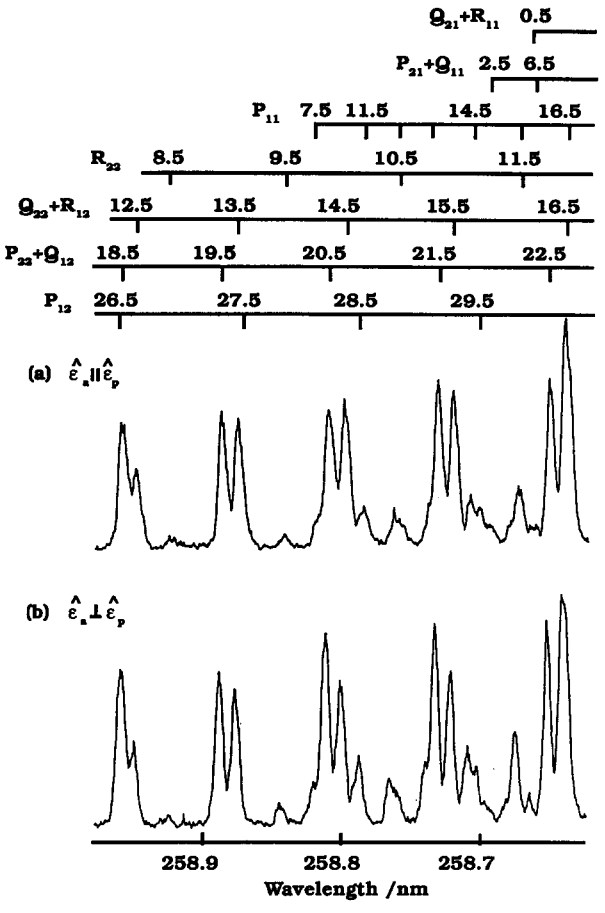

FIG. 2. An assigned portion of the NO(0–3) band following photolysis of HONO at 355 nm. The relative enhancement of the $Q_{22} + R_{12}$ branch in (a) with $\hat{\epsilon}_p \| \hat{\epsilon}_a$, and the $P_{22} + Q_{12}$ branch in (b) with $\hat{\epsilon}_p \perp \hat{\epsilon}_a$, indicates a positive rotational alignment.

Q dominated, branch is much stronger in Geometry I when $\hat{\epsilon}_p \| \hat{\epsilon}_a$, which is indicative of a positive value of the rotational alignment.

Spectra of NO($v'' = 1$) are somewhat more complicated by the presence of contributions from thermal NO and NO from NO_2. Figure 3 shows that population in $v'' = 1$ at high J'' can be attributed to nascent NO from HONO. Figures 3(a) and (b) are the short wavelength ends of spectra due to pure NO and NO_2 respectively, and Fig. 3(c) is a spectrum obtained from the HONO sample. Pure NO was prepared chemically using a standard technique [2] and purified by vacuum distillation: NO_2 was obtained commerically (BDH, 99.5%) and saturated with O_2 (BOC) before use. A spectrum identical to that shown in Fig. 3(a) although much less intense, was recorded from the HONO sample when operating with the probe laser beam only. NO($v'' = 1$) from NO_2 is seen to populate J'' up to $\sim$24.5 strongly and then fall off rapidly; evidence of $J'' = 36.5$ is just visible. The different intensity pattern and extent of structure in the spectrum of the HONO sample indicates a nascent NO($v'' = 1$) population from dissociation of HONO that peaks at $\sim J'' = 30.5$ and extends to $\sim J'' = 53.5$.

B. Etalon scans

Doppler profiles of single rovibronic transitions are potentially the most sensitive probe of the photodissociation dynamics. When the laser has sufficient resolution and the range of recoil velocities is narrow the Doppler profiles may allow the characterization of vector correlations. Even if the laser bandwidth is sufficiently large relative to the maximum recoil Doppler width such that the effects of vector correlations cannot be resolved, it is still possible to estimate the

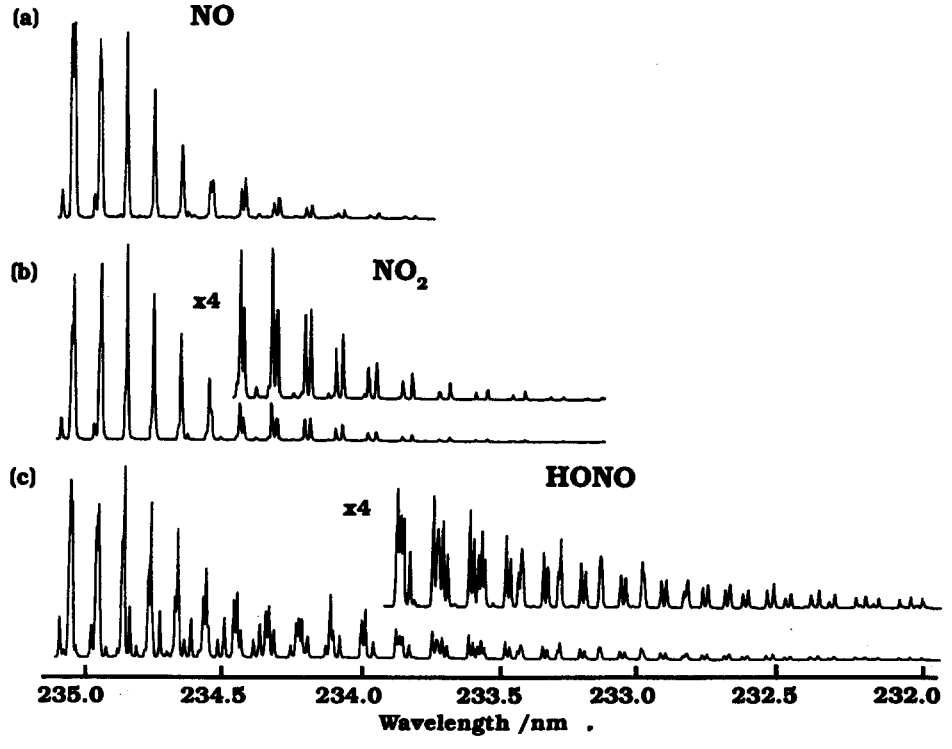

FIG. 3. The short wavelength (high J) end of the NO (0–1) band recorded (a) using pure NO, (b) from 355 nm photolysis of pure NO_2, and (c) from 355 nm photolysis of the HONO sample.

mean translational recoil energy through a measurement of the spectral widths. This serves as a diagnostic for the identity of the parent species because the measured width must be consistent with the available energy.

Our observed line shapes for NO(0–3) are distinctly non-Gaussian and are characterized by widths in the range 0.40–0.34 cm^{-1}. Measurements of the I_2 widths indicated the laser bandwidth to be $\sim$0.066 cm^{-1} in the visible (at $\sim$575 nm) and it has been anticipated that this would give $\sim$0.13 cm^{-1} in the UV. However, the cumulative effects of the frequency doubling and Raman-shifting processes resulted in a bandwidth estimated to be $\sim$0.18 cm^{-1} based on the measurement of NO(0–0) transitions in thermal NO. The laser bandwidth and parent thermal Doppler width ($\sim$0.07 cm^{-1} at this wavelength) were combined into a Gaussian profile which was convoluted with a rectangular recoil Doppler line shape for simulating spectral line profiles. This method provides approximate estimates of the maximum recoil widths for each line. The values of 0.31 ± 0.04 cm^{-1} thus deduced for $v'' = 3$ are comparable to the calculated maximum value of 0.34 cm^{-1} and consistent with HONO being the parent species. Measurement of NO(0–2) widths yield a recoil width of 0.42 ± 0.04 cm^{-1} which is again consistent with HONO as the precursor. The line shapes in NO(0–3) spectra taken in trial experiments using a pulsed nozzle were greater than 0.34 cm^{-1} and were distinctly peaked, indicating that the precursor under these conditions was not (bare) HONO.

C. Rotational alignment

The recorded intensities in the NO LIF excitation spectra must be corrected for the effects of rotational alignment, in order to determine rotational distributions. This naturally necessitates the determination of the alignment parameter $A_o^{(2)}$ which characterizes the (μ,J) correlation between the transition dipole μ in the parent, and the angular momentum J in the fragment. The simplest method of cancelling alignment effects is to normalize the intensities of spectra taken in different experimental geometries to the intensity of a transition for which $A_0^{(2)}$ is zero, such as $R_{21}(0.5)$. The inverted nature of the rotational distributions and spectral congestion rendered the measurement of low J'' transitions impractical and therefore the judicious normalization of spectra by this method was not possible. Consequently it was necessary to measure the areas of well resolved rovibronic transitions in both geometries I and II and to combine this data with the J and geometry-dependent multipliers b_0 and b_1, respectively, of the alignment parameters $\beta_0^0(00) \equiv A_0^{(0)}$ and $\beta_0^2(02) \equiv \frac{1}{4}A_0^{(2)}$[13] to obtain consistent values for the alignment and hence deduce rotational populations.

The NO(0–2) and NO(0–3) bands were rigorously analyzed to determine an average value of $A_0^{(2)}$ for $v'' = 2$ and 3, respectively. Each spectrum contained over 300 transitions which were, in places, heavily congested. As a total of four sections of spectrum were recorded for each geometry and vibrational band, a method was developed which computationally measured the areas of suitably resolved spectral transitions. The energies of all spectral transitions in the recorded region were generated from the known molecular constants of NO[14] and sifted through a computer algorithm to leave those transitions likely to be resolvable in the spectra, given the known Doppler broadened linewidths. The position of each resolved transition in turn on the composite spectra, such as that in Fig. 1, was predicted with respect to a known reference peak. The center of gravity was found iteratively and the area determined. Provided that the difference between the predicted and calculated positions was less than a preset threshold, the area and transition were recorded and the calculated position was used to refine the reference point before predicting the position of the next transition. This served to allow for nonlinearities in the dye laser grating drive and slight inaccuracies in the splicing together of spectra. Each recorded area was then divided by the appropriate line strength factor[15] for the transition to obtain an intensity dependent only on the ground state population, a mean alignment, and the alignment multipliers. The ability of this technique to accurately reproduce a known population distribution, in the absence of alignment, had been rigorously tested. A trial spectrum of NO(0–3) was computer simulated assuming a Gaussian distribution in the ground state rotational states centered at $J'' = 23$ with a width in J'' of 16. The populations derived from this in the above manner were found to yield precisely this input distribution. The total number of fully resolved transitions in the complete band is only $\sim$70.

For each integrated intensity, $I(G,Q_i)$, we may write

$$\frac{I(G,Q_i)}{CS_i(Q_i)} = N(Q_i)\{b_0(G,Q_i) + b_1(G,Q_i)\beta_0^2(02)(Q_i)\}, \tag{4}$$

where G refers to the geometry (I or II) and Q_i refers to the set of quantum numbers (J_i,Ω_i,Λ_i) which specify the ground rotational state which has a population $N(Q_i)$. S_i is the line strength of the probed transition and C is a constant. The left-hand side of Eq. (4) is the quantity calculated using the raw spectra and the b_0 and b_1 values on the right are known. Taking any two intensities referring to the same initial level enables the determination of $\beta_0^2(02) \equiv \frac{1}{4}A_0^{(2)}$ for the particular Q_i. This is fulfilled by different transitions in the same spectrum which originate from a common level or by the same transition in two different experimental geometries. Unfortunately, there are few such comparisons to be made of resolved transitions in the same spectrum and, in addition, where comparisons are possible the transitions are usually widely separated in frequency and have quite different line strengths. Hence variations in the uniformity of experimental conditions and any saturation effects have a pronounced effect on the derived value of $A_0^{(2)}$. Such variations are not, however, so important when comparing intensities of the same transition in two different geometries and because of the similarity of spectra there are many possible comparisons. The major problem here is to normalize the two spectra so that they represent the same ground state population. This is nontrivial as experiments were taken under different conditions on different days and separately normalized to the intensity of a chosen spectral feature.

The approach taken was to normalize data obtained from spectra in different geometries to a common total (inte-

grated) intensity and an average of four data sets was calculated. These were then scaled such that reliable comparisons between transitions in the same spectrum and between transitions in different geometries gave consistent values of $A_0^{(2)}$. Precisely the same scaling was applied to the $v''=3$ data as for $v''=2$ and the end results were encouragingly consistent. The calculation of the alignment involves taking the quotient of two, sometimes small, numbers and results in a large degree of error. For a particular transition in geometries $G=\mathrm{I}$ and $G=\mathrm{II}$ the rotational alignment is related to the intensities $I(G)$ by

$$\beta_0^2(02)=\frac{5}{4}A_0^{(2)}=\frac{b_0\{I(\mathrm{II})-I(\mathrm{I})\}}{\{b_1(\mathrm{II})I(\mathrm{I})-b_1(\mathrm{I})I(\mathrm{II})\}}, \quad (5)$$

where b_0 is the same in both geometry I and II and $b_1(\mathrm{I})$ and $b_1(\mathrm{II})$ are the respective b_1 multipliers in the two cases. The most reliable comparisons are, therefore, those for which there is a large difference in magnitude and a change in sign of the b_1 multiplier. The $Q_{22}+R_{12}$ and $P_{21}+Q_{11}$ branches offer the best opportunity for calculating $A_0^{(2)}$ when the experimental geometry is changed. These branches are relatively intense giving good signal-to-noise ratios. These two branches probe the antisymmetric $\Pi(A'')$ Λ doublet in the $F_2(^2\Pi_{3/2})$ and $F_1(^2\Pi_{1/2})$ manifolds, respectively. The probe power densities were kept low enough to minimize saturation effects.

The quality of the data, given the errors in taking areas of lines which may be slightly overlapped, and variations across the spectra, did not warrant the determination of $A_0^{(2)}$ as a function of J''. However, the $Q_{22}+R_{12}$ and $P_{21}+Q_{11}$ branches yield a mean value for the rotational alignment, $A_0^{(2)}$ which is the same for the $\Pi(A'')$ levels for both the F_1 and F_2 spin components within the fitted error. A combined fit of the F_1 and F_2 data for $v''=2$ gave

$$A_0^{(2)}(v''=2)=0.27\pm0.01;\ 8.5\leqslant J\leqslant 43.5. \quad (6)$$

The same procedure applied to the $v''=3$ data resulted in the value

$$A_0^{(2)}(v''=3)=0.26\pm0.01;\ 11.5\leqslant J\leqslant 38.5. \quad (7)$$

A similar calculation for the $\Pi(A')$ levels is hampered by small changes in b_1 and in intensity between the two geometries, and by branches whose low line strength factors magnify errors. We will assume that the corresponding $A_0^{(2)}$ values will be similar to those of the $\Pi(A'')$ levels. A detailed study of the dissociation of the closely related CH_3ONO molecules,[16] for example, reveals a mean rotational alignment independent of the Λ-doublet or spin-doublet components.

D. Rotational distributions

The mean value of the alignment for each v'' is now used to calculate the ground state rotational state populations $N(Q_i)$ using Eq. (4). Figure 4 shows $N(J'')$ plotted against J'' for the four Λ components in $v''=2$ and 3. The distributions are fitted with a Gaussian-type function of the form:

$$N(J)=h_m\exp\left[\frac{-4\ln 2(J-J_m)^2}{J_w^2}\right] \quad (8)$$

which is centered at J_m and has a full width at half-maximum J_w, and h_m is the height at J_m. Pairs of branches probe the same Λ doublet and these were least-squares fitted to produce the smooth line through the points. Figures 4(a) and 4(b) each combine the Gaussian profiles which characterize the rotational distributions in $v''=2$ and 3, respectively, on the same diagram. The data points are omitted for clarity. The inset shows an example of such a least-squares fit to populations derived from the experimental data. In this case the $P_{22}+Q_{12}$ (x) and R_{22} (Δ) branches were a probe of the rotational sublevels $F_{2f}(A')$, equivalent to $^2\Pi_{3/2}(A')$ of Fig. 4(a).

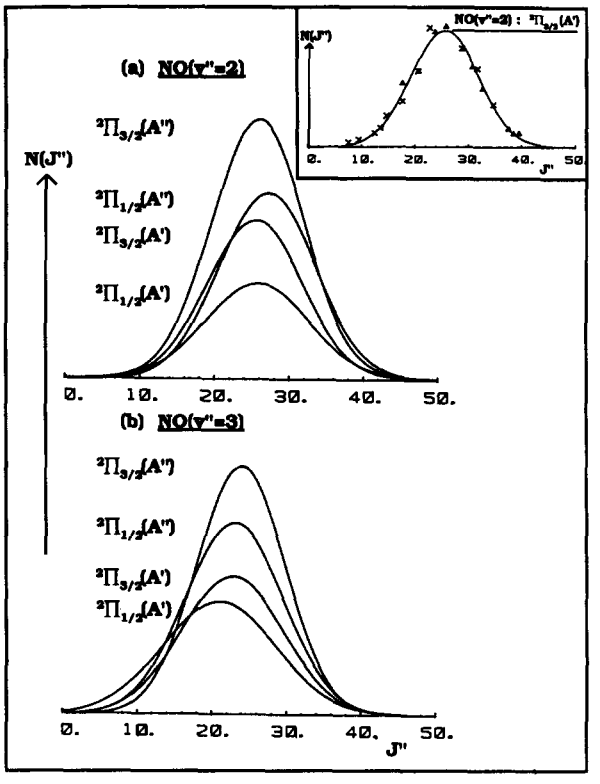

FIG. 4. Gaussian profiles characterizing the rotational state population distributions in each of the four sets of substates for (a) NO($v=2$) and (b) NO($v=3$) following photolysis of HONO at 355 nm. Inset: the fit of the least-squares Gaussian function to the experimental populations for the $F_{2f}(A')$ levels of NO($v=2$).

The four rotational distributions in each vibrational state are characterized by the following mean parameters:

$$J_m=25.9\pm0.5,\ J_w=15.2\pm0.9 \text{ in } v''=2, \quad (9)$$

$$J_m=22.6\pm0.7,\ J_w=15.5\pm1.5 \text{ in } v''=3. \quad (10)$$

The widths of the $v''=2$ and 3 distributions are the same within the error while the center of the distribution lies at higher J'' in lower v''. The parameters J_m and J_w of the $v''=1$ distribution in NO from HONO are difficult to determine due to the small number of transitions that are well resolved and not overly contaminated by the NO contribution from NO_2 dissociation. It is therefore necessary to concentrate on transitions at the short wavelength or high J end of the spectrum, which precludes a rigorous analysis. From a comparison of the pure NO_2 and HONO sample spectra it is estimated the J_m is ~ 30 for $v''=1$, with a width J_w comparable to those for $v''=2$ and 3.

The F_1 and F_2 fine structure components are not in equilibrium with one another: the spin distribution is inverted with the energetically higher $F_2(^2\Pi_{3/2})$ component more populated than the lower $F_1(^2\Pi_{1/2})$ component. There are few direct comparisons possible between data points with a common J'' and the same electronic reflection symmetry (A' or A'') and so we choose to characterize the spin distribution by the mean F_2/F_1 ratio of the $\Pi(A'')$ and $\Pi(A')$ levels at the peak of their respective distributions. We find:

$$F_2/F_1 \sim 1.4 \text{ in } v'' = 2\ (J \sim 26)$$

and

$$F_2/F_1 \sim 1.25 \text{ in } v'' = 3\ (J \sim 22). \tag{11}$$

The quality of the data limits the accuracy of this measurement, but the important result is that $F_2/F_1 > 1$.

The Λ-doublet populations are clearly anomalously populated. Figure 4 shows that $[\Pi(A'')] > [\Pi(A')]$ in both $v'' = 2$ and $v'' = 3$. Thus the unpaired electron preferentially occupies the $p\pi$ lobe which lies perpendicular to the plane of rotation of the NO at high J, $\pi(a'')$. These ratios do not simply reflect relative orbital populations, since the degree of orbital alignment (DEA), defined in Ref. 17 as

$$\text{DEA} = \frac{[\Pi(A'')] - [\Pi(A')]}{[\Pi(A'')] + [\Pi(A')]} \tag{12}$$

(but see also Ref. 44), is influenced by partial spin uncoupling which is strongly J dependent. Least-squares fits of the results from all possible comparisons between data points were performed and a mean value of the observed DEA for the population, independent of spin component, was obtained. The mean values were

$$\text{DEA} = 0.27 \pm 0.03 \text{ in } v'' = 2$$

and

$$\text{DEA} = 0.26 \pm 0.03 \text{ in } v'' = 3. \tag{13}$$

These values compare favorably with the mean values calculated from a comparison at the Gaussian maxima, of DEA = 0.28 and 0.27, respectively.

E. Vibrational distribution

An estimate was made of the relative populations in $v'' = 2$ and $v'' = 3$. This measurement is notoriously problematical because the bands which probe these states are widely separated in energy and require the use of different laser dyes to probe them. It is therefore difficult to maintain known and consistent conditions between measurements especially when, as in this case, the concentration of sample varies with time. The NO(0–3) and (0–2) bands were recorded in succession while still flowing the same HONO sample and maintaining the same gains on the signal and power detection. The falloff in HONO concentration was assumed linear over the time taken to interchange laser dyes so that the relative concentrations for the two spectra could be calculated. The variation in detection efficiency with wavelength of the PM and photodiode was neglected. The spectra were normalized to the power and corrected for HONO decay and their total areas measured, which were then scaled to reflect the mean signal level of each band. Taking the different transition probabilities for the two bands into account [the ratio (0–2):(0–3) is $\sim 1.5{:}1$[10]] it was estimated that

$$\frac{N(v'' = 3)}{N(v'' = 2)} \sim 0.01, \tag{14}$$

i.e., ~1% of NO occupies $v'' = 3$ relative to $v'' = 2$.

The determination of the $v'' = 1$ relative population is again complicated by the overlapping NO from NO_2 as noted in Sec. III D. As a "guesstimate" of this population we compared the intensities of the R_{22} lines aroung J_m for the $v'' = 1$ and $v'' = 2$ distributions. The power sensitivity remained unaltered between these measurements and it was assumed that the HONO concentration was the same for each. The comparison indicated that the population in $v'' = 1$ may be as much as twice that in $v'' = 2$, i.e.,

$$\frac{N(v'' = 1)}{N(v'' = 2)} \sim 2. \tag{15}$$

This estimate is supported by the improved signal-to-noise in the NO(0–1) spectra compared with that in NO(0–2) around their respective J_m values. Combining the results of Eqs. (14) and (15) it can be concluded, albeit tentatively, that

$$N(v'' = 1){:}N(v'' = 2){:}N(v'' = 3) = 2{:}1{:}0.01. \tag{16}$$

F. Energy partitioning

Having characterized the NO rotational distribution in $v'' = 2$ and 3, and estimated the rotational distribution in $v'' = 1$ and the vibrational distribution, the available energy in the dissociation E_{av} can be apportioned between the various degrees of freedom in both NO and OH. The mean translational energy has previously been measured[2] and conservation of momentum determines the mean NO translational energy. The OH rotational distribution $N(J)$ is close to Boltzmann with an effective temperature parameter of ~300 K, whereas the NO rotational distribution has a Gaussian functional form [Eq. (8)]. The mean energy in rotation $\langle E_r \rangle$ is given by

$$\langle E_r \rangle = \frac{\Sigma N(J) E_J}{\Sigma N(J)}, \tag{17}$$

where $E_j = BJ(J+1)$ approximates the rotational energy, B is the rotational constant, and the summation is over all occupied J'' levels. OH has no observed vibrational excitation and so the energy still unaccounted for is present in NO vibrational excitation.

It is further possible to construct the distribution functions $N_v(E)$ for the total internal energy of NO, at least to the extent that the uncontaminated data will allow. Figure 5 displays $N_v(E)$ for $v = 1, 2$, and 3 derived from the Gaussian parametrization of the rotational distributions [Eq. (8)], using the best fit values of Eqs. (9) and (10) for $v = 2$ and 3, respectively, and $J_m = 30.5$ with $J_w = 16$ for $v = 1$. The different normalization of $N(E)$ and $N(J)$ has been taken into account. This figure shows clearly that the rotational energy distribution narrows with increasing vibrational quantum number; and that after taking the vibrational distribution

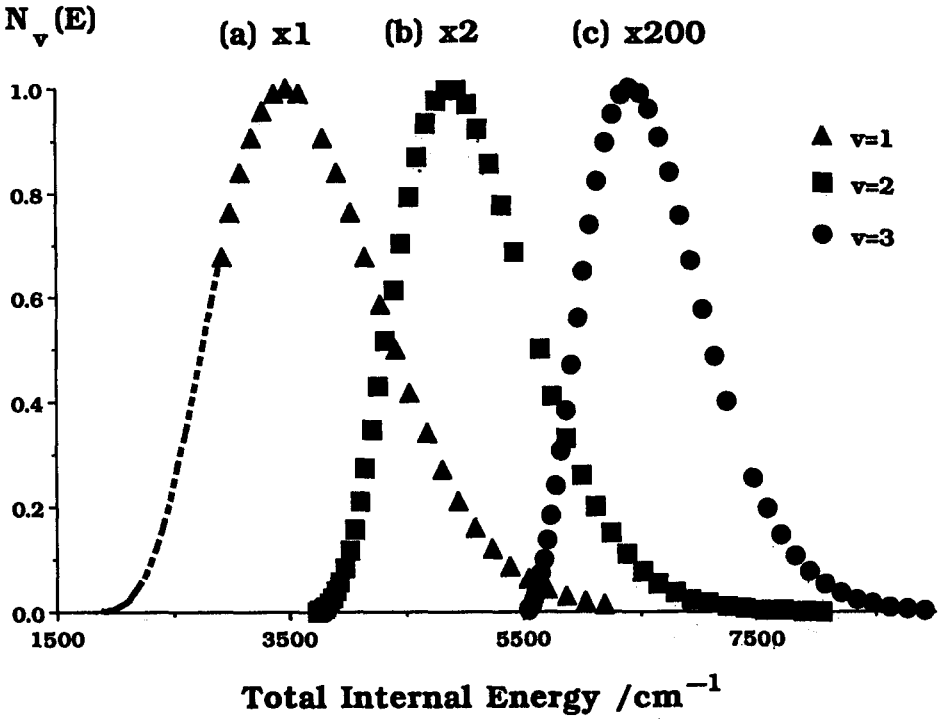

FIG. 5. The distribution functions $N_v(E)$ for the total internal energy of NO from HONO normalized and plotted separately for (a) $v=1$, (b) $v=2$, and (c) $v=3$. The dotted section of (a) is masked by interference from other sources of NO, and is drawn by extrapolation. The relative vibrational populations are given with the curves.

into account the overall width of the NO internal energy distribution is fairly narrow ($\sim$2000 cm^{-1}), apart from a high energy tail. This implies a narrow velocity distribution for OH, which is in accord with the earlier deductions from the profiles of the recoil-Doppler broadened OH lines.[1,2]

These results are summarized in Table I.

IV. DISCUSSION

HONO is the prototype for the alkyl nitrites RONO. Unlike HONO, the higher members of this series of compounds are chemically stable and may be prepared in a pure form devoid of NO or NO_2. As the C–O–N = O moiety in these molecules undergoes a dissociative $\pi^* \leftarrow n$ transition in the near UV and the NO fragment is such a sensitive probe of the dynamics, the RONOs ($R > H$) have been studied extensively.[18] We shall refer to the information available on CH_3ONO,[16,19–25] C_2H_5ONO,[26,27] $(CH_3)_3CONO$ or *t*-BuONO(tertiarybutylnitrite),[28,29] and the related $(CH_3)_2NNO$ or DMN (dimethylnitrosamine)[27,29–31] for comparison with the results of this work, as many aspects of the photodissociation dynamics will be common to all.

Rotational alignment

Table II collects together the experimentally determined values of rotational alignment (and recoil anisotropy parameters) for the RONO series. All values, including that for NO from HONO, are positive indicating that the angular momentum vector J tends to lie parallel to the transition moment μ of the parent molecule, which implies preferential population of $M \sim |J|$ in the magnetic sublevels. The general trend is a reduction in alignment with increasing size of R with the exception that the value of HONO appears to be anomalously low. The value of $A_0^{(2)}$ for HONO can be rationalized by considering the factors which contribute to the

TABLE I. Energy partitioning between NO and OH.[a,b]

	NO					OH	
	$v''=1$	$v''=2$	$v''=3$	$\langle E_q\rangle$/cm^{-1}[c]	$\frac{\langle E_q\rangle}{E_{av}}$%	$\langle E_q\rangle$/cm^{-1}	$\frac{\langle E_q\rangle}{E_{av}}$%
E_r	(1630)	1226	948	(1500)4430[d]	(13)38	210	2
E_v	1876	3722	5544	(2930)	(25)	...	...
E_t				2520	22	4490	38
E_{total}				6950	60	4700	40

[a] Energy available for partitioning $E_{av} = 11\,650$ cm^{-1}.

[b] Numbers in brackets are estimates based on the apparent $v''=1$ rotational distribution and/or assume the vibrational distribution in Eq. (16), i.e., $(v=0):(v=1):(v=2):(v=3) = 0{:}2{:}1{:}0.01$.

[c] $q = r$, v, t or total, as appropriate.

[d] $\langle E_{v+r}\rangle = 11\,650 - E_{total}(OH) - E_t(NO) = 4430$ cm^{-1}.

TABLE II. Fragment alignment $\{A_0^{(2)}\}$ and recoil anisotropy (β) parameters in the dissociation of RONO.[a]

RONO	J range	β	$A_0^{(2)}$	Ref.
	OH			
HONO	0.5–5.5	−0.8	0.1–0.3	2
	NO			
HONO	10.5–40.5		0.27	this work
CH_3ONO	20.5–40.5	−0.7	0.47	24,25
C_2H_5ONO	15.5–40.5	−0.7	0.38	24,26
$(CH_3)_3CONO$	30.5–45.5		0.32	28
	20.5–40.5		0.40	29
$(CH_3)_2NNO$	10.5–40.5	−0.56	0.1	27
	25.5–45.5		0.16	29,30

[a] Adapted and updated from Ref. 18.

reduction of the alignment from the limiting value of 0.8 at high J for a planar dissociation:

(i) Inherent internal motions in the parent, and thermal population in the internal degrees of freedom, i.e., HONO at room temperature has zero-point energy in its six normal modes of vibration and $\sim\frac{1}{2}kT$ in each degree of rotation about the principal axes. Upon dissociation these motions contribute to both parallel ($\|$) and perpendicular ($\perp$) rotational angular momentum of the ejected NO wth respect to the initial molecular plane. The major portion of NO rotational energy derives from the impulse along the breaking bond producing rotation in the plane. Nevertheless the $\perp$ component of angular momentum will reduce $A_0^{(2)}$ by a factor $\langle P_2(\mathbf{J}\cdot\mathbf{z})\rangle$, whereas in the absence of a $\perp$ contribution $\mathbf{J}$ would lie along the parent $z(\boldsymbol{\mu})$ axis in the classical limit of high J. This reduction will be present even when the dissociation is infinitely fast.

(ii) Following photopreparation of molecules with z along $\hat{\boldsymbol{\epsilon}}_p$, rotation of the parent framework about the principal axes due to a finite lifetme before fragmentation further reduces $A_0^{(2)}$ by $\langle P_2(\cos\phi)\rangle$, where ϕ is the angle through which the framework rotates in the lifetime τ.

Parent rotation appears in both contributions and will be significant in light parent molecules which have large rottional constants, especially if the dissociation is relatively slow.

The magntiude of effects (i) has been estimated for HONO, taking $E_r(\perp)\sim 100\,\mathrm{cm}^{-1}$ for the contribution made to NO rotation by the parent internal motions due to disappearing vibration and to rotation. This component relative to the measured $E_r(\|)\sim 1000\,\mathrm{cm}^{-1}$ reduces $A_0^{(2)}$ by a factor of

$$\langle P_2(\mathbf{J}\cdot\mathbf{z})\rangle_{\mathrm{NO}}\sim 0.85. \tag{18}$$

A similar calculation for the OH fragment with $E_r(\|)\sim 200\,\mathrm{cm}^{-1}$ and $E_r(\perp)\sim 100\,\mathrm{cm}^{-1}$ gives

$$\langle P_2(\mathbf{J}\cdot\mathbf{z})\rangle_{\mathrm{OH}}\sim 0.5. \tag{19}$$

Rotation of the parent molecule about its a and b axes leads to a further reduction in alignment if there is a finite time for dissociation, since fragmentation then takes place with respect to a rotated plane of reference [rotation about the axis of the transition dipole ($\mathbf{c}$) does not cause disalignment]. We associate the further factor required to reproduce the observed NO alignment with this second effect, and use it to deduce a lifetime. This requires that the time dependent factor have the value

$$\langle P_2(\cos\omega\tau)\rangle\approx 0.4. \tag{20}$$

Since the parent molecules are in Boltzmann equilibrium at ~ 300 K we have assumed Gaussian distributions for the angular velocities about the $\mathbf{a}$ and $\mathbf{b}$ axes, with mean energy $\frac{1}{2}kT$ in each. For an assumed τ the rms angles of rotation ϕ_a^0 and ϕ_b^0 were calculated, and the expectation value calculated by numerical integration. In this way we find that

$$\tau = 110\ \mathrm{fs};\ \phi_a^0 = 45°;\ \phi_b^0 = 14°. \tag{21}$$

The calculated lifetime is certainly an average value of a distribution of times, but nevertheless should accord with the value of the lifetime responsible for the observed reduced value for recoil anisotropy parameter β of the OH fragment from HONO.

The reduction of β from its limiting value of -1 can be regarded as recoil at an angle θ_t less than 90°, i.e.,

$$\beta = \langle 2P_2(\cos\theta_t)\rangle \tag{22}$$

with θ_t the angle between $\boldsymbol{\mu}$ and $\mathbf{v}(\mathrm{OH})$. For OH this gives an average recoil angle of $|90° - \theta_t|\approx 15°$. Alternatively, for the planar dissociation the reduction in β can be attributed to $\perp$ components of recoil velocity imparted through internal motions of the parent and rotation during a finite lifetime, i.e., (i) and (ii) above. Following the analysis of Busch and Wilson[32] which assumes a first order lifetime of parent decay and neglects the contribution of parent vibrational momentum to $\perp$ velocity, we calculate a value for the lifetime of ~ 80 fs. This value from OH is in fairly good agreement with the value obtained from the analysis of the alignment of NO.

Despite the assumptions and approximations made in rationalizing the alignment it is clear that there are several contributions whose significance is determined by the size and geometry of the molecule, the lifetime of the excited state and the temperature of the surroundings. The major reduction of $A_0^{(2)}$ in NO from HONO arises from parent rotation about in-plane axes, even though the lifetime is relatively short. CH_3ONO and the higher RONOs are less affected by rotation; for example the A rotational constant of

$CH_3ONO(\tilde{X})$ is a factor of 4.5 less than that of $HONO(\tilde{X})$[33] and accordingly CH_3ONO has a higher observed alignment. As the size and complexity of R increases down the series we expect an increased contribution from parent vibrations, especially from the torsion about the O–N bond. This, coupled with a slight increase in parent lifetime might explain the reduction in $A_0^{(2)}$ from CH_3ONO to DMN.

If the assumption about the contributions from parent rotation through both transferred angular momentum and finite lifetime is correct, we might expect to observe a more limiting value for the alignment from a jet-cooled sample, where only the lowest few levels of parent rotation are populated. The effect in HONO should be pronounced, but unfortunately cluster formation under jet conditions has prevented such a measurement. Rotational alignment of NO from jet-cooled CH_3ONO has been measured[21] and the value of $A_0^{(2)} = 0.56$ is slightly higher than the room temperature value of $A_0^{(2)} = 0.47$,[24] and a similar effect has been observed in H_2O.[34] These observations confirm the presence of a contribution made by parent rotation to the reduction in the alignment from its limiting value.

An argument similar to that above is equally applicable to the rotational alignment of OH from HONO. Consideration of the contributions made by internal motions and the same value of the lifetime of $\tau = 110$ fs yields an expected value of $A_0^{(2)} = 0.16$. This indeed lies within the observed range (Table II).

Λ doublets, spin doublets, and the influence of spin uncoupling in $^2\Pi$ states

The Λ-doublet and spin-doublet populations of the $NO(X\,^2\Pi)$ fragment show a distinct preference for the unpaired electron to occupy the $\pi(a'')$ orbital and with its spin coupled to $^2\Pi_{3/2}$. The maximum values possible for these two internal alignments are strongly influenced by the transition from Hund's case (a) at low J towards Hund's case (b) at high J.

Complete $\pi(a')$ or $\pi(a'')$ specificity is only manifest as complete Λ-doublet specificity (DEA $= \pm 1$) in case (b). Andresen and Rothe[17] have taken intermediate coupling into account, and have given numerical values for the expected maximum degree of electron alignment (DEA) for both $NO(X\,^2\Pi)$ and $OH(X\,^2\Pi)$. The experimental values for NO [Eq. (13)] should be compared with the limiting values of ± 0.56 for $J = 25.5$ and ± 0.52 for $J = 22.5$. Thus for both the $v'' = 2$ and $v'' = 3$ fragments the observed DEA is ~ 0.48 of that for pure $\pi(a'')$ specificity. A similar analysis of the $OH(X\,^2\Pi)$ $v'' = 0$ fragment shows that the observed DEA for $N = 4$–6^2 is 0.55 ± 0.1 of that possible for the opposite pure $\pi(a')$ specificity. It if is assumed that the dynamics of the ensemble of parent molecules leads to $\pi(a'')$ and $\pi(a')$ orbital occupancies that are uncorrelated, then

$$\frac{[\pi(a'')] - [\pi(a')]}{[\pi(a'')] + [\pi(a')]} = \frac{(\mathrm{DEA})_{\mathrm{obs}}}{(\mathrm{DEA})_{\mathrm{max}}}. \tag{23}$$

The observed values then correspond to relative $\pi(A''):\pi(a')$ orbital occupancies of 2.8:1 for NO and 1:3.4 for OH, respectively.

In contrast, complete spin alignment in the molecular frame only leads to pure F_1 or F_2 specificity in Hund's case (a). The limiting values possible for a degree of spin alignment (DSA);

$$\mathrm{DSA} = \frac{[F_1] - [F_2]}{[F_1] + [F_2]}, \tag{24}$$

occur when the dynamics leads to the exclusive excitation of either the $^2\Pi_{1/2}$ or $^2\Pi_{3/2}$ basis functions. This limit for the DSA is given in terms of the well known coefficients for intermediate coupling[17] as $\pm (a_J^2 - b_J^2)$. For NO this takes the value ± 0.81 for $J = 25.5$ and ± 0.84 for $J = 22.5$. The observed values of DSA $= -0.17$ for $v'' = 2$ and -0.11 for $v'' = 3$ are only ~ 0.2 of the extreme for pure $^2\Pi_{3/2}$ specificity.

In OH the transition from case (a) to case (b) is very rapid with increasing J. It has been found that F_2 is again more populated than F_1 at the lowest J, with the difference diminishing almost to zero by $N = 6$.[2] The DSA values at low N (-0.25 for $N = 1$) are only 0.2–0.3 of those for the extreme of pure $^2\Pi_{1/2}$. Thus although some spin alignment is found in both the NO and OH fragments, in both cases this is far smaller than might occur for an adiabatic correlation to one coupled pair of spin–orbit states.

These results are summarized in Table III along with those for other nitrites. In all cases there is a small positive DEA indicating a bias towards the A'' Λ doublets. The small extents of spin alignment are more erratic. For a planar dissociation to $OH^2\Pi + NO^2\Pi$ the generation of spin alignment requires spin–orbit mixing between the initially prepared $\tilde{A}\,^1A''$ state and states of $^3A'$ symmetry. An *ab initio* calculation predicts a $^3A'$ state higher than the $\tilde{A}$ state near the equilibrium HONO geometry, but with a potential function dropping below that for the $\tilde{A}$ state as they both converge to ground state products.[35] The extent of spin alignment can be expected to be a very sensitive function of the dynamics in this long range region, much dependent on the time of interaction and thus masses, velocities and precise trajectories.

Since the degree of Λ-doublet specificity is low in all the molecules in Table III this is unlikely to be the result of torsional or rotational motion of the parents, as these have widely varying masses and vibration frequencies. However, we note that the planar combination of ground state products can give rise to two $^1A''$ configurations. In a valence-bond coupling scheme for HONO these are

$$OH(^2\Pi A') + NO(^2\Pi A'') \rightarrow HONO(^1A''), \tag{25a}$$

and

$$OH(^2\Pi A'') + NO(^2\Pi A') \rightarrow HONO(^1A''). \tag{25b}$$

In the same coupling scheme the ground state arises from

$$OH(^2\Pi A') + NO(^2\Pi A') \rightarrow HONO(^1A'), \tag{26}$$

thereby forming the central ON σ band for the *trans*-bent equilibrium geometry. The conventional $\pi^* \leftarrow n(NO)$ description of the first nitrite absorption then corresponds to excitation from Eq. (26) to Eq. (25a). Dissociation from such a state would lead to high values of the DEA in both fragments, with $(\pi a')(\pi a'')^2$ on OH and $(\pi)^4(\pi^* a'')$ on NO. However, since Eqs. (25a) and (25b) are degenerate at

TABLE III. Degree of electron alignment and spin–orbit population ratios for nascent NO from RONO ($\tilde{A}$).[a]

RONO	$\nu(N=0)/\text{cm}^{-1}$[b]	PR[c]	DEA[d]	F_1/F_2[e]
(free $N=O$	1876[k]	1	0	1.83[f])
HO–N = O[g]	1698[l]	1.74	0.27	0.75
		(OH: 0.47	−0.36	0.60)[o]
CH_3O–N = O[h]	1681, 1625(*cis*)[m]	1.50	0.2	1.17
C_2H_5O–N = O	1670[m]			
$(CH_3)_3CO$–N = O[i]	1655[m]	~1.50	0.2	1.56
$(CH_3)_2N$–N = O[i,j]	1439[n]	1.15	0.07	1

[a] DEA estimated at $J'' = 25.5$, for which maximum possible DEA = 0.56.
[b] Values for *trans*-RONO except where indicated.
[c] $PR = \Pi(A'')/\Pi(A')$.
[d] $DEA = (PR - 1)/PR + 1)$.
[e] Average values of $^2\Pi_{1/2}/^2\Pi_{3/2}$.
[f] Calculated for 300 K using a spin–orbit splitting constant A for $\sim 126\ \text{cm}^{-1}$.
[g] This work.
[h] Reference 24.
[i] Reference 29.
[j] Reference 27.
[k] Reference 36.
[l] Reference 4.
[m] Reference 37.
[n] Reference 38.
[o] OH values from Ref. 2; F_1/F_2 here is $^2\Pi_{3/2}/^2\Pi_{1/2}$ as OH is inverted. Maximum |DEA| for $N \sim 4$ is ~0.55. Thermal $F_1/F_2 = 1.96$ ($A \sim -140\ \text{cm}^{-1}$) at 300 K.

long range we may anticipate some configuration mixing at short range, so that the electronic excitation includes a contribution from Eq. (26) → Eq. (25b). Upon dissociation this leads to $(\pi a')^2(\pi a'')$ on OH and $(\pi)^4(\pi^* a')$ on NO, corresponding to the *opposite* signs of the DEA in *both* products. We therefore propose that configuration interaction (or delocalization in an MO model) is the main cause of low degrees of Λ-doublet specificity in all the nitrites.

Nuclear dynamics and the potential energy surface

The vibrationally structured nature of the HONO ($\tilde{A}$–$\tilde{X}$) absorption spectrum is an indication that the nature of the potential energy surface inhibits direct dissociation, thereby permitting some recurrence of the evolving $\tilde{A}$ state wave function within the Franck–Condon region. This is borne out by our estimates of 80 or 110 fs for the parent lifetime deduced from vector correlations; 100 fs corresponding to a Lorentzian linewidth of 53 cm^{-1} which is comparable with the HONO experimental bandwidths. Nevertheless, the high fraction of the available energy appearing as product recoil (60%) attests to the impulsive nature of the eventual fragmentation for excitation at 355 nm.

Let us first consider the rotational excitation of the NO. The simplest model of the dissociation is that of an impulse acting directly along the breaking ON bond. The torque from such an impulse would generate an NO rotational energy of 2170 cm^{-1}.[2] This is nearly 50% higher than the value observed (Table I), and this model is also incapable of accounting for the low degree of OH rotation. We therefore seek a less extreme picture of the dynamics.

An NO molecule accelerated from rest to $J = 30.5$ in 50 fs would have been rotated by only about 28° (which is probably an upper limit). We can therefore rationalize the observed partitioning between translation and rotation of NO by considering the impulsive force generated by the breaking bond to act from the OH fragment at some mean impact parameter $\bar{b}$ to the center of mass of NO (see Fig. 6). We assume that this force is responsible for the linear momentum of the recoiling fragments and the angular momentum of the NO, to give the observed translational and rotational energies, and that, even though the force must be a function of elapsed time, it drops to zero over a short range of OH–NO separation R. From this pseudo-triatomic model we derive:

$$\bar{b} = a\bar{R}/\sqrt{a^2 + \bar{R}^2} \tag{27a}$$

with

$$a = \left[\frac{\mu_{NO}}{\mu_{HO\text{-}NO}} \cdot \frac{E_{rot}}{E_{tr}}\right]^{1/2} r_{NO} \tag{27b}$$

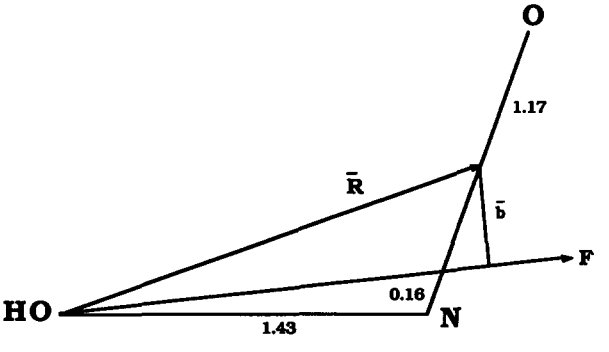

FIG. 6. Dissociation of HONO as a pseudo-triatomic molecule. The mean repulsive force F acts from the O atom of OH at an angle to the ON bond, with mean impact parameter $\bar{b}$ to the center of mass of NO. $\bar{b}$ is chosen to reproduce the observed partitioning between translational recoil and NO rotation for each vibrational state of NO. Distances is Angstroms.

Applying this equation to the results of Table I, separately for each v''(NO), with an assumed $\bar{R}$ of 1.75 Å taken from the molecular geometry, leads to

$$v''(\mathrm{NO}) = 1;\ \bar{b} \approx 0.42\ \text{Å} \tag{28a}$$

$$v''(\mathrm{NO}) = 2;\ \bar{b} = 0.40\ \text{Å} \tag{28b}$$

$$v''(\mathrm{NO}) = 3;\ \bar{b} = 0.41\ \text{Å} \tag{28c}$$

using the mean values of E_{rot}(NO) for each v''. If the force had acted directly through the N atom $\bar{b}$ would have been 0.58 Å based on the ground state structural parameters. Thus we can describe the force as acting at an angle of about 6° to the O–N bond through a point about 0.16 Å along the N = O bond, as shown schematically in Fig. 6. This is compatible with a tendency for the ONO angle to increase towards linearity during the initial states of dissociation. The near constancy of $\bar{b}$ shows that the lowering of E_{rot} with increase in v'' is a simple consequence of the reduction in the energy available for partition between translation and rotation.

The Gaussian form of the NO rotational distributions, and their widths, are directly related to the initial momentum distribution for the zero-point motion of the ONO bending vibration of HONO, for which $\nu_5'' = 598\ \mathrm{cm}^{-1}$.[4] Using the same pseudo-triatomic HO–N–O model as above,[2] the kinetic energy of this disappearing mode is reflected in a Gaussian distribution of –NO rotational angular momentum with a calculated full width at half maximum of

$$J_w = 17, \tag{29}$$

using entirely ground state parameters. Relaxation of ν_5'' towards a lower ν_5' before dissociation would tend to lower J_w. Thus the observed values of $J_w \sim 15$–16 [Eqs. (9) and (10)] are fully compatible with this simple model.

The NO vibrational distribution is a more complex function of the potential energy surface for the HONO $\tilde{A}\,^1A''$ excited state. In the earlier discussion of the observations of the OH fragment[2] it was suggested that this surface may be rather flat along r_{ON} near the Franck–Condon region, but repulsive further out. The vibrational structure of the HONO absorption spectrum would then be associated with this localized pocket of quasi-stability. *Ab initio* calculations have recently confirmed this suggestion,[39,40] and predict a shallow well around a *trans* structure having $r_{\mathrm{HO}} = 0.95$ Å, $r_{\mathrm{ON}} = 1.34$ Å, $r_{\mathrm{NO}} = 1.35$ Å, HON = 105.1° and ONO = 104.5°. Very small distortions of the ONO angle eliminate the well, leaving only a point of inflection on the surface as a function of the bondlengths.[41] The shortened ON bond in the excited state (cf. $r'' = 1.44$ Å) may be a consequence of the configuration interaction discussed above in connection with Eq. (25).

Dissociation from the inner well proceeds via a transition state with $r_{\mathrm{ON}} = 1.50$ Å and $r_{\mathrm{NO}} = 1.27$ Å, thereby involving a concerted motion in both these coordinates. A further feature of the surface is that the force constant for NO motion increases with lengthening of the ON bond, as it tends towards the higher force constant of free NO. It is therefore not surprising that the observed NO vibrational distribution is far from that predicted earlier on the basis of a simple Franck–Condon (sudden) model for the single terminal NO vibration.[2]

Hennig *et al.*[9] have carried out a number of classical and quantum calculations of the product NO vibrational distribution using their *ab initio* surface, and three different two-dimensional approximations to the full six-dimensional dynamics. While there are substantial differences in the quantitative predictions from these various calculations, they do focus attention on two basic mechanisms. As for CH_3ONO,[42] the main vibrational structure in HONO is associated with a vibration which is mainly that of the terminal $N = 0$ bond, but also involves a smaller in-phase amplitude of ON stretching. This v_2' mode is given the quantum number n^* in Ref. 39.

Adiabatic dissociation resulting in $v(\mathrm{NO}) = n^*$ is hindered by the necessity of tunneling through the low barrier at the transition state. Furthermore, the increase in N = O force constant along the exit channel causes the barrier in the one-dimensional adiabatic potential corresponding to $v = n^*$ to increase with increasing n^*, since $\nu_2' \sim 1100\ \mathrm{cm}^{-1}$ and $\nu(\mathrm{NO}) \sim 1876\ \mathrm{cm}^{-1}$. In the calculations of Ref. 39 this adiabatic dissociation mechanism is of very minor importance except for $n^* = 0$.

The dominant mechanism in the calculations is that of vibrationally nonadiabatic transitions from level n^* to a lower level, mainly $n^* - 1$, induced by kinetic energy coupling. By this IVR (intramolecular vibrational redistribution) mechanism the energy of one or more quanta of n^* vibration is used to surmount the barrier in a lower adiabatic curve, leading to $v(\mathrm{NO}) = n^* - 1$ or $n^* - 2$. The matrix elements promoting this mechanism will increase with increasing n^*.

Our observations show less dominance of the IVR mechanism with $n^* = 2 \rightarrow v = 2$ being about one half of the probability of $n^* = 2 \rightarrow v = 1$, rather than of negligible importance. We have observed the same trend for photolysis at 369 nm via $v_2(n^*) = 1$,[43] with higher average NO vibrational energy than predicted in Ref. 39. The interpretation above of the deduced impact parameter $\bar{b}$ suggests that angle-bending motions cannot be completely neglected in a quantitative treatment of the energy disposal. Thus the use in Ref. 39 of a cut of the potential for a fixed ONO angle may not include the route of steepest descent through the transition state, thereby overemphasizing the barriers in the one-dimensional adiabatic potentials. We can anticipate that the relative importance of the adiabatic and IVR mechanisms will be highly sensitive to the heights of any such barriers.

V. CONCLUSION

The observations described in this paper on the NO fragment from HONO ($\tilde{A}\,^1A''$) photodissociation are complementary to those presented earlier for the OH fragment.[2] Taken together they give a very complete picture of the overall process for this prototypical four atom system. In many ways this dissociation resembles that of a pseudo-triatomic molecule: the small extent of the excitation of the OH fragment is carried over from its initial motion within the parent molecule, whereas the NO is subject to strong excitation forces. This is seen to be a direct consequence of negligible

structural changes between the OH of HONO and free OH, but major changes in bonding for the NO. The dissociation is slow enough, and the exit channel sufficiently tortuous, that exit channel effects have an important controlling influence on the energy disposal within the NO; but is too fast to permit any equilibration between NO and OH.

ACKNOWLEDGMENTS

We are indebted to the Science and Engineering Research Council for financial support. We also thank K. N. Rosser and C. M. Western for advice and assistance.

[1]R. Vasudev, R. N. Zare, and R. N. Dixon, Chem. Phys. Lett. **96**, 399 (1983).
[2]R. Vasudev, R. N. Zare, and R. N. Dixon, J. Chem. Phys. **80**, 4863 (1984).
[3]R. Varma and R. F. Curl, Jr., J. Phys. Chem. **80**, 402 (1976).
[4]G. W. King and D. Moule, Can. J. Chem. **40**, 2057 (1962).
[5]R. D. Kenner, F. Fohrer, and F. Stuhl, J. Phys. Chem. **90**, 2635 (1986).
[6]R. A. Cox, J. Photochem. **3**, 175 (1974).
[7]R. A. Cox and R. G. Derwent, J. Photochem. **6**, 23 (1976/77).
[8]F. A. Cotton and G. W. Wilkinson, *Advanced Inorganic Chemistry*, 3rd ed. (Wiley, New York, 1972).
[9]S. Gerkenstorn and P. Luc, *Atlas du Spectre D'Absorption de la Molecule D'Iode* (CNRS, Paris, 1978).
[10]L. G. Piper and L. M. Cowles, J. Chem. Phys. **85**, 2419 (1986).
[11]H. Zacharias, M. Geilhaupt, and K. H. Welge, J. Chem. Phys. **74**, 218 (1981).
[12]H. L. Johnston and W. F. Giauque, J. Am. Chem. Soc. **51**, 3194 (1929).
[13]R. N. Dixon, J. Chem. Phys. **85**, 1866 (1986).
[14]W. G. Mallard, J. H. Miller, and K. C. Smyth, J. Chem. Phys. **76**, 3483 (1982).
[15]L. T. Earls, Phys. Rev. **48**, 423 (1935).
[16]U. Bruhlmann and J. R. Huber, Chem. Phys. Lett. **143**, 199 (1988).
[17]P. Andresen and E. W. Rothe, J. Chem. Phys. **82**, 3634 (1985).
[18]H. Reisler, M. Noble, and C. Wittig, in *Molecular Photodissociation Dynamics*, edited by M. N. R. Ashfold and J. E. Baggott (Royal Society of Chemistry, London, 1987).
[19]O. Benoist D'Azy, F. Lahmani, C. Lardeux, and D. Solgadi, Chem. Phys. **94**, 247 (1985).
[20]F. Lahmani, C. Lardeux, and D. Solgadi, Chem. Phys. Lett. **102**, 523 (1983).
[21]F. Lahmani, C. Lardeux, and D. Solgadi, Chem. Phys. Lett. **129**, 24 (1986).
[22]P. Felder, B. A. Keller, and J. R. Huber, Z. Phys. D **6**, 185 (1987).
[23]U. Bruhlmann and J. R. Huber, Z. Phys. D **7**, 1 (1987).
[24]U. Bruhlmann, M. Dubs, and J. R. Huber, J. Chem. Phys. **86**, 1249 (1987).
[25]B. A. Keller, P. Felder, and J. R. Huber, J. Phys. Chem. **91**, 1114 (1987).
[26]A. F. Tuck, J. Chem. Soc. Faraday Trans. 2 **5**, 689 (1977).
[27]M. Dubs, U. Bruhlmann, and J. R. Huber, J. Chem. Phys. **84**, 3106 (1986).
[28]D. Schwartz-Lavi, I. Bar, and S. Rosenwaks, Chem. Phys. Lett. **128**, 123 (1986).
[29]R. Lavi, D. Schwartz-Lavi, I. Bar, and S. Rosenwaks, J. Phys. Chem. **91**, 5398 (1987).
[30]R. Lavi, I. Bar, and S. Rosenwaks, J. Chem. Phys. **86**, 1639 (1987).
[31]R. Lavi and S. Rosenwaks, J. Chem. Phys. **89**, 1416 (1988).
[32]G. E. Busch and K. R. Wilson, J. Chem. Phys. **56**, 3626 (1972).
[33]P. H. Turner, M. J. Corkill, and A. P. Cox, J. Phys. Chem. **83**, 1473 (1979).
[34]P. Andresen, G. S. Ondrey, B. Titze, and E. W. Rothe, J. Chem. Phys. **80**, 2548 (1984).
[35]C. Larrieu, A. Dargelos, and M. Chaillet, Chem. Phys. Lett. **91**, 465 (1982).
[36]G. Herzberg, *Molecular Spectra and Molecular Structure*, Vol. I (Van Nostrand, New York, 1950).
[37]P. Tarte, J. Chem. Phys. **20**, 1570 (1952).
[38]I. W. Levin, G. W. A. Milne, and T. Axenrod, J. Chem. Phys. **53**, 2505 (1970).
[39]S. Henning, A. Untch, R. Schinke, M. Nonella, and J. R. Huber, Chem. Phys. **129**, 93 (1989).
[40]H. U. Suter and J. R. Huber, Chem. Phys. Lett. **155**, 203 (1989).
[41]J. R. Huber (private communication).
[42]S. Hennig, V. Engel, R. Schinke, M. Nonella, and J. R. Huber, J. Chem. Phys. **87**, 3522 (1987).
[43]R. N. Dixon and H. Rieley Chem. Phys. (in press).
[44]M. H. Alexander, P. Andresen, R. Bacis, R. Bersohn, F. J. Comes, P. J. Dagdigian, R. N. Dixon, R. W. Field, G. W. Flynn, K.-H. Gericke, E. R. Grant, B. J. Howard, J. R. Huber, D. S. King, J. L. Kinsey, K. Kleinermanns, K. Kuchitsu, A. C. Luntz, A. J. McCaffery, B. Pouilly, H. Reisler, S. Rosenwaks, E. W. Rothe, M. Shapiro, J. P. Simons, R. Vasudev, J. R. Wiesenfeld, C. Wittig, and R. N. Zare, J. Chem. Phys. **89**, 1749 (1988).